Lab-on-a-chip platforms based on highly sensitive nanophotonic Si biosensors for single nucleotide DNA testing

J. Sánchez del Río[a], L.G. Carrascosa[a], F.J. Blanco[b], M. Moreno[a], J. Berganzo[b], A. Calle[a], C. Domínguez[a] and L. M. Lechuga[a]
[a]Biosensors Group. Microelectronics National Centre (CNM). CSIC. E-28760. Madrid (Spain)
[b]IKERLAN S.Coop. MEMS Department. E-20500 Mondragón (Guipúzcoa), Spain.

Abstract.

In order to solve the drawbacks of sensitivity and portability in optical biosensors we have developed ultrasensitive and miniaturized photonic silicon sensors able to be integrated in a "lab-on-a-chip" microsystem platform. The sensors are integrated Mach-Zehnder interferometers based on TIR optical waveguides ($Si/SiO_2/Si_3N_4$) of micro/nanodimensions. We have applied this biosensor for DNA testing and for detection of single nucleotide polymorphisms at BRCA-1 gene, involved in breast cancer development, without target labeling. The oligonucleotide probe is immobilized by covalent attachment to the sensor surface through silanization procedures. The hybridization was performed for different DNA target concentrations showing a lowest detection limit at 10 pM. Additionally, we have detected the hybridization of different concentrations of DNA target with two mismatching bases corresponding to a mutation of the BRCA-1 gene. Following the way of the lab-on-a-chip microsystem, integration with the microfluidics has been achieved by using a novel fabrication method of 3-D embedded microchannels using the polymer SU-8 as structural material. The optofluidic chip shows good performances for biosensing.

Keywords: Biosensor, Mach-Zehnder interferometer, Silicon microtechnology, DNA biosensing, microfluidics, lab-on-a-chip microsystem

1. INTRODUCTION

Evanescent wave photonic biosensor devices based on standard microelectronics and related micro/nanotechnologies are providing an integrated technological solution for achieving high sensivity arrays of biosensing devices. These evanescent wave sensors show a great potential for sensing biomolecular interactions in real-time without labeling requirements, which have made them quite useful for applications ranging from biomedical, environmental, industrial to genomic and proteomics. But problems of stability, sensitivity and size have prevented the general use of optical biosensors for real field applications.

The evanescent field is the part of the guided light that travels through a region that extends outward; around a hundred of nanometers, into the media surrounding the waveguide (see Figure 1). When there is a change in the optical characteristics of the outer medium (i.e. refractive index change or a biochemical reaction), a modification in the optical properties of the guided wave (phase velocity) is induced via the evanescent field. Optical evanescent wave biosensing techniques allow the direct monitoring of small changes in the optical properties. The direct detection method is not as sensitive as indirect ones (i.e. fluorescence, radiolabeling or enzyme amplification) but it requires, generally, no prior sample preparation and can be used in real time evaluations allowing the determination of concentration, kinetic constants and binding specificity of biomolecules.

Silicon Photonics II, edited by Joel A. Kubby, Graham T. Reed, Proc. of SPIE Vol. 6477
64771B, (2007) · 0277-786X/07/$18 · doi: 10.1117/12.713977

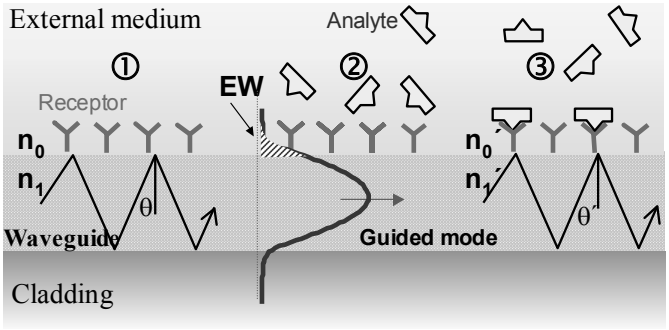

Fig. 1. Biomolecular interaction sensing by the evanescent wave detection principle in an optical waveguide sensor

For evaluation of specific interactions, the receptor is covalently attached to the sensor surface, while the complementary molecule binds to the receptor from free solution. The recognition of the complementary molecule by the receptor causes a change in the refractive index and the sensor monitors that change. After the molecular interaction, the surface can be regenerated using a suitable reagent in order to remove the bound analyte without denaturing the immobilized receptor.

Within the integrated evanescent wave sensors, the interferometric are the most promising due to their high sensitivity and capacity of integration. Several interferometric devices have been described, e.g., the Young interferometer [1,2] or the Mach-Zehnder interferometer (MZI), which is the most commonly employed for biosensing [3]. The MZI biosensor has been used for different applications such as gas detection [4], environmental pollutant analysis [5,6] and the detection or study of the interaction between proteins [7,8].

In order to solve the drawbacks of sensitivity and portability, we work on the development of ultrasensitive and miniaturized photonic sensors able to be integrated in a "lab-on-a-chip" microsystem platform. As sensors we use integrated Mach-Zehnder interferometer based on TIR optical waveguides ($Si/SiO_2/Si_3N_4$) of micro/nanodimensions. In a step towards such lab-on-a-chip microsystems, we have integrated the MZI device with the microfluidics using a novel fabrication method of 3-D embedded microchannels using the polymer SU-8 as structural material [9]. Multilevel optofluidic biosensor arrays have been successfully fabricated.

2. NANOPHOTONIC INTERFEROMETER DESIGN

In an integrated Mach-Zehnder interferometric device [10] the light traveling within a channel waveguide is divided in two arms, the sensing arm and the reference arm by means of a Y-divisor (see Fig. 2). These arms are recombined again, after a certain distance, producing the interference of both beams. In the sensor arm there is a region, called the sensor area, in which the evanescent field of the guided light can interact with the environment. The local changes of refractive index produced in the sensor area will induce a phase difference between the light beams traveling in both arms, which will be traduced as a change in the interference signal of the MZI device. Therefore, the output signal of the MZI is given by the following expression:

$$I_T = I_S + I_R + 2\sqrt{I_S I_R}\cos\Delta\varphi_S \tag{1}$$

where I_S and I_R are, respectively, the intensity of the light in the sensor and reference arms of the MZI, and $\Delta\varphi_S$ is the phase difference between the light traveling in both arms.

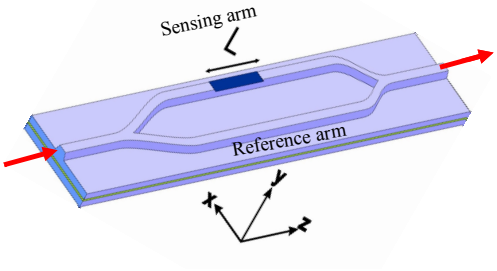

Fig. 2. Mach-Zehnder interferometer configuration

For biosensing applications, the optical waveguides of the integrated MZI must achieve two main characteristics: to have a high surface sensitivity and single mode behavior. Modelisation of the structure has been done based on silicon-related materials and visible wavelength. In order to evaluate the surface sensitivity (η_{sup}), we calculate the variation of the effective propagation index (N) [13] of the guided modes when the thickness of a homogeneous biological layer (d_l) changes,

$$\eta_{sup} = \frac{\partial N}{\partial d_\ell} \tag{2}$$

In Figure 3 we represent such surface sensitivity as a function of the core thickness, assuming that the refractive index of the biological layer is n_b = 1.45, the external medium is water (n_e = 1.33), and the light wavelength is 632 nm. We can observe that the highest surface sensitivity is obtained in waveguides with a high contrast of refractive index between the core and the substrate [11] and maximum surface sensitivity is achieved for core thicknesses about 150 nm and 75 nm for the TM and TE polarizations, respectively. After the modelisation of the single-mode behavior for bilateral confinement of the light, the structure that has been finally chosen, for an operating wavelength of 0.633 μm, is the following: Silicon substrate; a 2 μm thick silicon dioxide cladding (n=1.46) and a silicon nitride core layer with a refractive index of 2.00 and thickness of 200 nm. Single mode behavior is obtained for core thickness below 200 nm, and rib depths below 4 nm when the rib width is 4 μm [11]. Figure 3 shows a scheme of the waveguide configuration. An extensive discussion on the modelisation can be found in [6].

To obtain couplers with low losses, the MZI configuration was designed where the Y-junction is shaped with circular bend. The final device has a length of 3 cm and the sensor area is 1.5 cm long and 50 μm wide. The length of the sensor area has been chosen as a compromise between the sensitivity of the device, which is proportional to the length of the sensor area, and the optical loses and portability of the final device.

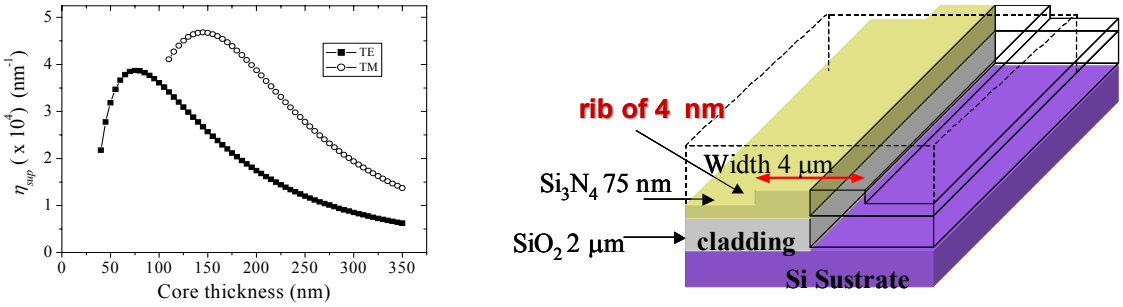

Fig. 3. *(left)* Theoretical surface sensitivity versus waveguide core thickness *(right)* TIR waveguides configuration employed for the MZI sensor

3. FABRICATION AND CHARACTERIZATION OF THE MZI DEVICES

The devices are fabricated in the Clean Room facilities as described previously [6]. After fabrication, the chips are diced and polishing for optical evaluation. The evaluation was performed in an optical bench where polarized light from a He-Ne laser (λ=0.633 μm) was end-fire coupled to the sensor by means of a 40x microscope objective. The light coming out the interferometer is collected by a single-mode fiber, which is pigtailed to a PIN photodiode (Figure 4). The photodiode signal is amplified, digitalized and processed in a PC. Precise translation stages are used for the accurate alignment of all the components.

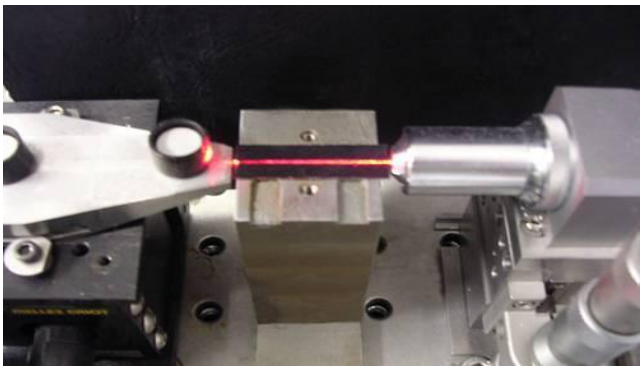

Fig. 4. Optical bench for MZI nanodevice characterization

Propagation losses of the waveguides were measured by the Fabry-Perot resonance technique [15] and optical coupling losses were calculated by the cut-back method [16]. Propagation losses, in the case of MZIs of 200 nm core thickness, vary between 0.13 and 0.15 dB/cm for TE polarization and between 0.27 and 0.30 dB/cm for TM polarization. The fiber-waveguide insertion loss measurements were 5.84 dB for TM polarization and 3.12 dB for TE polarization and low losses were assured with couplers designed with circular arms of R = 80 mm.

4. SENSITIVITY EVALUATION

The sensitivity of the sensor for both polarizations was evaluated in the same way as in previous reports [6]. The evaluation was done flowing solutions of water and ethanol of varying concentration and, therefore, different refractive index (steps of 10^{-3}), and measuring the output signal of the MZI in real time. With these measurements, a calibrating curve was obtained where the phase response of the sensor is plotted versus the variation in the refractive index. The experimental sensitivity measured for this device is $\frac{d\Delta\phi(2\pi)}{dn}$ = 4057 for TM polarization and $\frac{d\Delta\phi(2\pi)}{dn}$ = 1377 for TE polarization and are in agreement with theoretical sensitivities calculated using the effective index method. These values correspond to a surface sensitivity around $\frac{\partial\Delta\phi(2\pi)}{\partial d_l} = 2\cdot10^{-4}$ nm^{-1}.

The standard deviations (σ_v) and thermal drifts of the experimental set-up were evaluated in maximum condition of stability and considering the case in which the interferometric devices were located in the quadrature point. Under these conditions, the lowest detection limit in the phase change was calculated assuming the $3\cdot\sigma_v$ criterion, resulting in a value of $\Delta\varphi = 1.6\text{x}10^{-4}\text{x}2\pi$ rads for TM polarization. Taking account the signal-to-noise ratio of this configuration, the lowest detection limit in the variation of the refractive index was found to be (for TM polarization) $\Delta n_{0,\,min} = 1\cdot10^{-7}$ ($\Delta N_{eff,\,min} = 6.4\cdot10^{-8}$).

5. DNA BIOSENSING

As a proof of the utility of MZI technology towards biosensing detection, the application of the MZI nanobiosensors for the direct detection of DNA is described. The first step is the immobilization of the oligonucleotide receptor in the sensor area. This immobilization must be strong and stable to perform sensitivity measurements and for ensure the reusability. For that reason, a covalent immobilization protocol through self assembled monolayers using silane chemistry is employed. Immobilization requires the previous cleaning of the Si_3N_4 surface with oxygen plasma and 10% nitric acid in distilled water to oxidize the surface. Secondly, the silicon nitride layer is immersed in a 10% 3-mercaptopropyltrimethoxysilane (MPTMS) in toluene at room temperature for 12 hours. The sensor surface is functionalized with a silane that has a thiol group at the free end. In this way, the thiol-derivatized oligonucleotides (28 mer) used as receptors can bind to the silanized Si_3N_4 surface through a disulphide bond. After DNA immobilization, complementary oligonucleotides (58 mer) were flowing in the sensor for hybridization experiments. 50 mM phosphated buffered (PB) solution, pH=7 and 0.75 M NaCl was used for both immobilization and hybridization experiments. The oligonucleotides sequences employed in the experiments are shown in Table 1.

Concentrations from 1 pM to 1 μM of the MR and WT oligonucleotides in buffered solution were flowed along the sensor area of the MZI and hybridized with the immobilized monolayer. To test that no change in the phase response was obtained when the oligonucleotide sequence is not complementary, different concentrations of the MF oligonucleotide in buffered solution were flowed. Regeneration after each hybridization was achieved flowing DI water and HCl 3.2 mM.

Table 1. Immobilization, complementary and non complementary oligonucleotide sequences. The WT oligonucleotide has the same complementary sequence than the BRCA-1 gen and MR has two punctual mutations, which are involved in inherited breast cancer predisposition. This last sequence is complementary to the SH oligonucleotide that was previously immobilized on the sensor area.

IMMOBILIZATION SEQUENCE (SH)	**5'-SH-$(CH_2)_6$-** TTT TTT TTT TTT TTT **GTT CTG TCA AACT – 3´**
WILD TYPE SEQUENCE (WT)	5´- TGC CAC ATG GCT CCA CAT GCA **AGT TTG AAA CAG AAC** TAC CCT GAT ACT TTT CTG GAT GCC -3´
MUTATED SEQUENCE (MR)	5' – TGC CAC ATG GCT CCA CAT GCA **AGT TTG ACA GAA C**TA CCC TGA TAC TTT TCT GGA TGC C – 3'
CONTROL SEQUENCE (MF)	5´- GGC ATC CAG AAA AGT ATC AGG GTA GTT CTG TTT CAA ACT TGC ATG TGG AGC CAT GTG GCA – 3´

Figure 5 (a) shows the real time detection of the covalent immobilization of 100 nM SH-oligonucleotide, which gives a phase change of $\Delta\varphi_S = 6.2x2\pi$ rad. This value corresponds to a surface coverage of $\Gamma = 4.87$ pg/mm^2. Figure 5 (b) shows the real time detection of the hybridization event between the oligonucleotide MR 100 nM, MR 50 nM and control MF 1 μM and the immobilized probes, inducing a total phase change $\Delta\varphi_S = 2.75x2\pi$ rad (Γ=2.02 pg/mm^2), $\Delta\varphi_S = 1.2x2\pi$ rad (Γ=0.92 pg/mm^2), and $\Delta\varphi_S = 0$ rad, respectively.

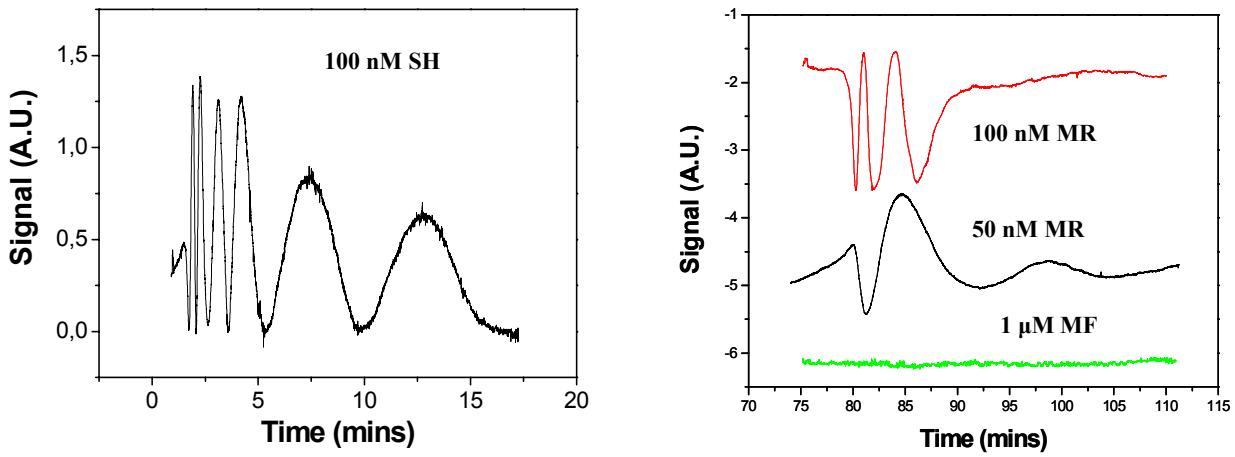

a) b)

Fig.5. a) Signal corresponding to the SH oligonucleotide 100 nM immobilization b) hybridization signals when MR 100 nM, MR 50 nM and control 1 μM are flowing in the sensor area.

A MZI calibration curve was obtained from 1 pM to 1 μM concentrations of the oligonucleotides MR, WT and MF control. Each oligonucleotide concentration data was taken three times and averaged to a mean value. The calibration curves are shown in Figure 6. The lowest detection limit is 10 pM with a phase change of $\Delta\varphi = 0.08x2\pi$ that means an estimation of a surface coverage of Γ=0.06 pg/mm^2 and a density of 1.5x10^6 molecules hybridized on the sensor area of the MZI.

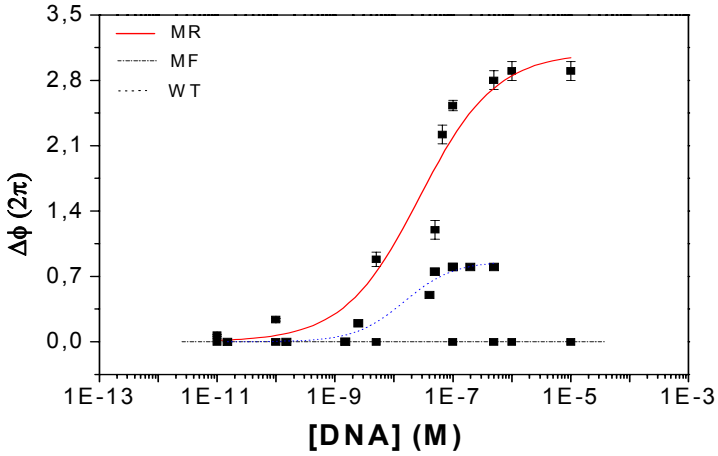

Fig. 6. Hybridization calibration curves for different concentrations of the oligonucleotides MR, WT and control.

So far most of the studies related to the direct detection of DNA hybridizations with optical biosensors have been performed using SPR biosensors [17-19]. The detection limit of the hybridization is above 10 nM. The results presented in Figure 6 set a 10 pM direct detection limit (without labeling) of DNA hybridization with the integrated MZI. Optimization of the covalent immobilization of the DNA probes and further lab-on-a-chip integration are expected to reduce the limit of detection to the fM range.

6. MICRO FLUIDICS INTEGRATION

For the development of a complete lab-on-a-chip microsystem device based on integrated MZI, several units must be incorporated on the same platform: (i) the micro/nanodevices, (ii) the flow cells and the flow delivery system, (iii) a phase modulation system to convert the periodic interferometric signals in direct phase measurements, (iv) integration of the light sources and the photodetectors (v) CMOS processing electronics. For achieving this goal, our first step has been the development of a novel low temperature (100 ºC) CMOS compatible microfluidic technology to create 3D embedded interconnected microfluidic channels between different substrates [20]. The microfluidic channels have a height from 40 to 60 μm and a width between 100 to 250 μm. In Figure 7 (a), photographs of the cross section of the channels and the water filling of the sensing area in the MZI devices can be observed. As a preliminary result, Figure 7 (b) shows the detection of a refractive index change of 6x10^{-4} using the integrated SU8 microfluidics.

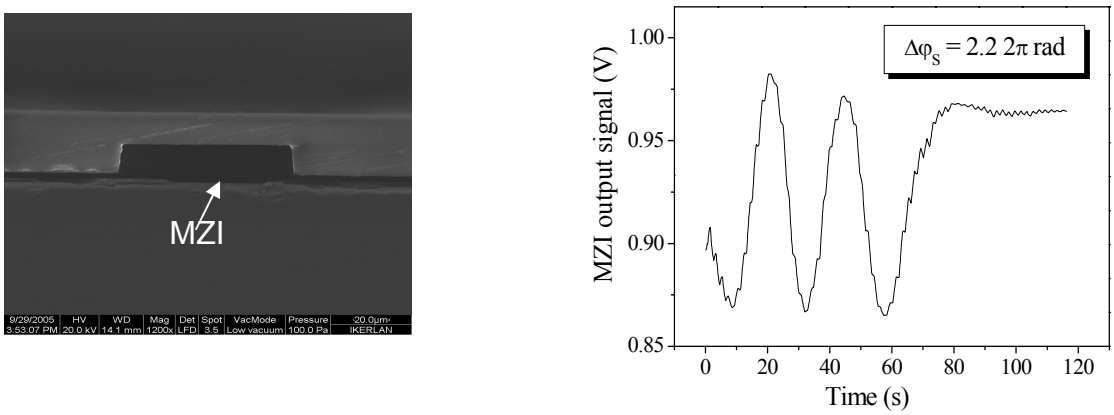

a) b)

Fig. 7. a) SEM photograph of the cross section of the SU8 microfluidic channels b) Detection of a refractive index change of $6 \cdot 10^{-4}$ using the integrated microfluidics.

7. CONCLUSIONS

We have presented the development of highly sensitive micro/nano optical biosensor devices based on integrated MZI. These sensors offer the capability to be integrated in lab-on-a-chip portable microsystems fully compatible with the CMOS standard technology. The interferometric devices have been applied in the label free and real time detection of DNA hybridization as well in the detection of single mutations. Following the way of the lab-on-a-chip microsystem, we have shown the integration of the microfluidic system using photolithographic patterned SU8 polymeric layers.

REFERENCES

1. A. Brandenburg , et al. "Interferometric sensor for detection of surface-bound bioreactions", *Applied Optics* 39**,** 6396-405 (2000).
2. Brynda E, et al, "Optical biosensors for real-time measurement of analytes in blood plasma", *Biosensors & Bioelectronics* 17 665-75, (2002).
3. R. G. Heideman, et al. "Remote opto-chemical sensing with extreme sensitivity: design, fabrication and performance of a pigtailed integrated optical phase-modulated Mach-Zehnder interferometer system", *Sensors and Actuators B* 61 100-27 (1999).
4. A. Brandenburg, et al. "Integrated Optical Gas Sensors Using Organically Modified Silicates as Sensitive Films", *Sensors and Actuators B* 11 361-74 (1993).
5. B. Drapp, et al. "Integrated optical Mach-Zehnder interferometers as simazine immunoprobes", *Sensors and Actuators B* 39 277-82 (1997).
6. F. Prieto, et al. "An integrated optical interferometric nanodevice based on silicon technology for biosensor applications", *Nanotechnology* 14 907-12 (2003).
7. F. Brosinger, et al. "A label-free affinity sensor with compensation of unspecific protein interaction by a highly sensitive integrated optical Mach-Zehnder interferometer on silicon", *Sensors and Actuators B* 44 350-5 (1997).
8. F. Prieto, et al. "Integrated Mach-Zehnder interferometer based on ARROW structures for biosensor applications", *Sensors and Actuators B* 92 151-8 (2003).

9. F. J. Blanco, M. Agirregabiria, J. Garcia, J. Berganzo, M. Tijero, M. T. Arroyo, J. M. Ruano, I. Aramburu and K.Mayora. "Novel three dimensional embedded SU-8 microchannels fabricated using a low temperature full wafer adhesive bonding" *Journal of Micromechanics and Microengeeniring* 14 1047-1056 (2004).
10. O. Parriaux, G.J. Veldhuis, "Normalized analysis for the sensitivity optimization of integrated optical evanescent-wave sensors," *J. Lightwave Technol.,* vol. 16, pp. 573-582 (1998).
11. E.F. Shipper, A.M. Brugman, C. Domínguez , Lechuga, L.M, Kooyman, R.P.H. & Greve, J., "The realization of an integrated Mach-Zehnder waveguide immunosensor in silicon technology" *Sensors and Actuators B*, vol. 40, pp. 147-153 (1997).
12. T. Tamir, *Guided-wave optoelectronics*, Springer, Berlin (1988).
13. K. Okamoto. *Fundamental of Optical waveguides*. Optics and Photonics (2003).
14. J. Sánchez del Río et al. "Integrated interferometric biosensor based on optical waveguides CMOS compatible", *Proceed. Eurosensors XIX,* Spain (2005).
15. R. Regener, et al. "Loss in low-finesse TI-$LiNbO_3$ optical wave-guide resonators" *Appl. Phys. B* 36 143-147 (1985).
16. I.P. Kaminow and L.W. Stultz, "Loss in cleaved Ti-diffused $LiNbO_3$ waveguides" *Appl. Phys. Lett.* 33 N1, 62-64 (1978).
17. Piscevic D, et al. "Oligonucleotide Hybridization Observed by Surface-Plasmon Optical Techniques", *Applied Surface Science* 90, 425-36 (1995).
18. Kai E, et al. "Detection of PCR products in solution using surface plasmon resonance" *Analytical Chemistry* 71 796-800 (1999).
19. Jiang T S, et al. "Detection of TP53 mutation using a portable surface plasmon resonance DNA-based biosensor" *Biosensors & Bioelectronics* 20 1939-45 (2005).
20. F. J. Blanco et al. "Microfluidic-optical integrated CMOS compatible devices for label-free biochemical sensing", *Journal of Micromechanics and Microengineering,* 16, 1006-1016 (2006)